

**Motions of the substrate recognition duplex in a group I intron assessed by site-directed spin-labeling**

Gian Paola G. Grant<sup>1</sup>, Nathan Boyd<sup>2</sup>, Daniel Herschlag<sup>2</sup>, and Peter Z. Qin<sup>1\*</sup>.

<sup>1</sup>Department of Chemistry, University of Southern California, Los Angeles, California 90089-0744; <sup>2</sup>Department of Biochemistry, Stanford University, Stanford, California 94305-5307.

**Supporting Information**

## S.I. Materials and Methods

### RNA preparations

Sequences and nomenclatures of ribozyme and oligonucleotides used in this study are listed in Table S1 and S2, respectively. All RNA oligonucleotides were chemically synthesized by Integrated DNA Technologies, Inc. (Coralville, IA) and were deprotected by the vendor.

The secondary structure of the L-16 *ScaI* ribozyme is shown in Figure S1. A five-nucleotide extension at the 5'-end of the L-16 *ScaI* ribozyme distinguishes its Internal Guidance Sequence (IGS) from that of the L-21 *ScaI* ribozyme (1). Forward primers (Integrated DNA Technologies, Inc., Coralville, IA.) containing the desired sequences of L-16 *ScaI* ribozyme constructs (Table S1) were used to PCR-amplify DNA from a plasmid encoding the wild type ribozyme. DNA was transcribed using a modified version of the standard protocol for *in vitro* transcription designed to avoid endonucleolytic cleavage of L-16 RNA (1-3). Briefly, reactions were allowed to proceed for 40 min at 30 °C in 4 mM MgCl<sub>2</sub>, 0.5 mM each NTP, 40 mM DTT, 40 mM Tris, pH 8.1, 0.01% Triton X-100, 5 µg/mL L-16 *ScaI* DNA template, and 2 mM Spermidine. RNA was ethanol precipitated and RNeasy Maxi (QIAGEN) column-purified according to the manufacturer's specifications. RNA constructs were 5'-[γ-<sup>32</sup>P]-ATP labeled and sequences were validated by denaturing PAGE subsequent to T1 RNase digest.

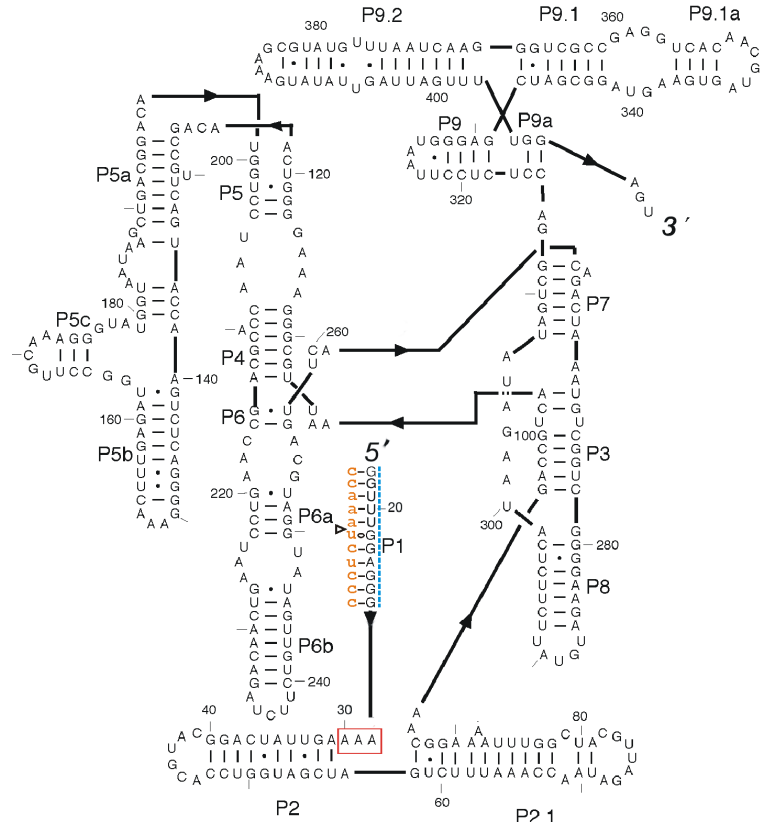


**Figure S1:** The secondary structure of the L-16 *ScaI* ribozyme. The paired regions are indicated by P. The red box marks the J1/2 element, and the dotted blue line shows the internal guide sequence (IGS). The substrate oligonucleotide is shown in orange, and the cleavage site is marked by the triangle.

**Table S1: 5'-Termini of the L-16 *ScaI* constructs used in this study.**

Construct	IGS	J1/2
L-16 (Wild Type)	GGUUUGGAGGG	AAA
-3A	GGUUUGGAGGG	----
+5A	GGUUUGGAGGG	AAAAAAA

**Table S2. Substrate oligonucleotides used to measure dissociation rate constants ( $k_{off}$ ).**

	Abbreviation	Sequence	Purpose
1.	rS	rCrCrC rUrCrU rArArA rCrC	Chase
2.	S <sub>C</sub> <sup>SL</sup>	rCrCrC rUrCdU rAdA*rA rCrC	Promotes closed complex Spin labeled (S <sub>p</sub> diastereomer)
3.	S <sub>O</sub> <sup>SL</sup>	rCrCrC mUrCrU rAdA*rA rCrC	Promotes open complex; Spin labeled (S <sub>p</sub> diastereomer)
4.	rS <sub>C</sub>	rCrCrC rUrCdU rArArA rCrC	Promotes closed complex; Not spin labeled
5.	rS <sub>O</sub>	rCrCrC mUrCrU rArArA rCrC	Promotes open complex; Not spin labeled
6.	S <sub>C</sub> <sup>SL(-)</sup>	rCrCrC rUrCdU rAdArA rCrC	Promotes closed complex; Not spin labeled; Control for assessing effect of the deoxyribose modification at the labeling site
7.	S <sub>O</sub> <sup>SL(-)</sup>	rCrCrC mUrCrU rAdArA rCrC	Promotes open complex; Not spin labeled; Control for assessing effect of the deoxyribose modification at the labeling site

r: 2'-OH

d: 2'-H

\*: R5a spin label (see Fig. 1A of main text)

m: 2'-OCH<sub>3</sub>*Nitroxide labeling*

The nitroxide precursor, 4-bromo-3-bromomethyl-2,2,5,5-tetramethyl-1-oxylpyrroline, was kindly provided by Dr. Kálmán Hideg (University of Pécs, Hungary). A typical labeling reaction mixture (50  $\mu$ L) included approximately 700  $\mu$ M of crude, phosphorothioate modified RNA, 100 mM of nitroxide precursor, 100 mM MES (pH 5.8), and 50% (v/v) acetonitrile. The solution was incubated overnight at room temperature in the dark with constant mixing.

After nitroxide coupling, the labeled product was first purified by anion-exchange HPLC, then desalted using a G-25 Sephadex column. The anion-exchange HPLC procedure removed excess nitroxide precursor and unwanted RNA fragments, separated the R<sub>p</sub> and S<sub>p</sub> diastereomers of the nitroxide-labeled oligonucleotide, and revealed the absolute diastereomeric configurations. The exact details of the anion-exchange HPLC procedure has been reported elsewhere (4).

Desalted oligonucleotides were lyophilized, re-suspended in ME (10 mM MOPS, pH 6.5, 1 mM EDTA), and stored at  $-20$  °C. The final concentration of the labeled oligonucleotides was determined by its absorption at 260 nm. The extinction coefficients of the unmodified oligonucleotides were used, as neither the phosphorothioate modification nor the nitroxide significantly alters the absorbance at 260 nm.

*Thermal denaturation of nitroxide labeled RNA substrate duplexes*

The RNA substrate and its complementary strand (1.5  $\mu\text{M}$  in 400  $\mu\text{L}$ ) was dissolved in 50 mM sodium phosphate buffer (pH 6.8), heated to 95  $^{\circ}\text{C}$  for 2 min, and annealed in 100 mM NaCl for 1 hour. Melting transition curves were obtained using a DU800 UV-Vis spectrometer (Beckman Coulter, Fullerton, CA). Sample absorbance was measured at 260 nm for every 1  $^{\circ}\text{C}$  or 0.5  $^{\circ}\text{C}$  interval as temperature was increased from 25 to 85  $^{\circ}\text{C}$ . Melting curves fitting and free energy calculations were carried out as previously described (5).

*Dissociation rate constants ( $k_{\text{off}}$ ) of spin-labeled and control substrates*

Dissociation rate constants were measured with ribozyme in excess of 5'-[ $\gamma$ - $^{32}\text{P}$ ]-labeled oligonucleotide substrates according to a native-gel pulse-chase protocol previously described (6,7). Ribozyme (400 nM) was folded at 50  $^{\circ}\text{C}$  in 50 mM NaMOPS, pH 7.0, and 10 mM  $\text{MgCl}_2$  for 30 min. Radiolabeled oligonucleotide substrates (Table S2) were then individually incubated with L-16 *ScaI* RNA at 50  $^{\circ}\text{C}$  such that final solution conditions were 50 mM NaMOPS, pH 7.0 and 50 mM  $\text{MgCl}_2$ . An unlabeled 'chase' oligonucleotide (10  $\mu\text{M}$ ) was added at time zero ( $t_0$ ) to prevent reassociation of dissociated radiolabeled oligonucleotide, thus initiating the reaction. At designated times (0.25, 0.5, 3, 8, 20, 60, 120 min) an aliquot of each reaction was removed, added to a glycerol-based loading dye solution, and immediately and carefully loaded onto a chilled and running 24% acrylamide, non-denaturing gel in THEM buffer (33 mM Tris, 67 mM HEPES, 1 mM EDTA, 10 mM  $\text{MgCl}_2$ , pH 7.2, 4  $^{\circ}\text{C}$ ). To determine complete binding, a mock chase (buffer and  $\text{MgCl}_2$ ) was added instead of chase. Chase was also added prior to labeled substrate to determine the efficacy of the chase. Gels were dried and then imaged and analyzed using ImageQuant analysis software (Molecular Dynamics). Pulse-chase data were found to fit well with a first order exponential decay with  $R^2$  values of  $\geq 0.98$ .

*Assembly of nitroxide-labeled ribozyme-substrate complexes*

Nitroxide labeled substrate oligonucleotides (0.39 – 0.84 nmoles) were assembled with pre-folded ribozymes (10% in molar excess as compared to the substrate) in 600  $\mu\text{L}$  buffer A (50 mM NaMOPS, pH 6.5, and 10 mM  $\text{MgCl}_2$ ). To pre-fold the ribozyme, ribozyme was added to buffer A, incubated first at 50  $^{\circ}\text{C}$  for 30 min, then at room temperature for 10 min. The nitroxide labeled substrates were preheated at 95  $^{\circ}\text{C}$  for 2 min, then added directly to the pre-folded ribozyme. The ribozyme/substrate mixture was incubated for another 10 min at room temperature, then filtered through a membrane concentrator (Millipore Inc, MWCO 30 kD) to reduce the sample volume to 12–20  $\mu\text{L}$ . This step also removed free substrates and/or any trace amount of unattached spin-labels. The concentrated sample (10-60  $\mu\text{M}$  substrate/ribozyme complex) was used directly in EPR measurements.

*Continuous-wave EPR spectroscopy measurements*

EPR spectra were obtained using 5 – 10  $\mu\text{L}$  of samples placed in glass capillaries (1.0  $\times$  1.2 mm) sealed at one end. X-band EPR spectra were acquired on a Bruker EMX Spectrometer using a high sensitivity cavity (ER 4119HS, Bruker Biospin, Inc.). The incident microwave power was 2 mW, the field modulation was 1.0 or 1.5 G at a 100 kHz frequency. Sample temperatures were

set at 25 °C using a liquid nitrogen variable temperature setup. For each sample, 60 – 100 scans were collected and averaged. All EPR spectra were baseline corrected and normalized to the same number of spins using software kindly provided by the Hubbell group at UCLA.

### *Simulation of EPR spectra*

Simulations of nitroxide spectra were carried out using the *microscopic ordered macroscopic disordered* (MOMD) program developed by Freed and coworkers (8,9). The program uses an order parameter ( $S$ ) and an effective correlation time ( $\tau$ ) to describe the nitroxide diffusive motion under the restraint of an ordering potential. It has been used to analyze spectra from proteins (10), RNA (5,11,12), and DNA (13). Details regarding the MOMD model, the simulation parameters, and the fitting procedures have been reported (8,14).

Simulations reported here used basis set truncation parameters of  $L_{\text{emx}} = 20$ ,  $L_{\text{omx}} = 19$ ,  $K_{\text{mx}} = 8$ ,  $M_{\text{mx}} = 2$ ,  $\text{IPN}_{\text{mx}} = 2$ . The  $g$  and  $A$  tensors were set to previously used values ( $g_z = 2.0023$ ,  $g_x = 2.0076$ ,  $g_y = 2.0050$ ;  $A_z = 35.0$ ,  $A_y = 5.9$ , and  $A_x = 7.5$ ) (11). The number of allowed MOMD orientations ( $N_{\text{MOMD}}$ ) was set to 10. Rotational diffusion tensors ( $R_x$ ,  $R_y$ ,  $R_z$ ), diffusion tilt angles ( $\alpha_D$ ,  $\beta_D$ ,  $\gamma_D$ ), the orienting potential coefficients ( $c_{20}$ ), and the Gaussian inhomogeneous broadening magnetic parameter ( $\text{gib2}$ ) were varied to obtain best fit to the experimental spectra. The following values were used to obtain simulated spectra shown in Fig. 2 of main text: for -3A,  $c_{20} = 2.01$ ,  $R_x = 10^{7.95} \text{ s}^{-1}$ ,  $R_y = 10^{8.22} \text{ s}^{-1}$ ,  $R_z = 10^{8.51} \text{ s}^{-1}$ ,  $\alpha_D = 2.8^\circ$ ,  $\beta_D = 43^\circ$ ,  $\gamma_D = 53.4^\circ$ , and  $\text{gib2} = 1.00$ ; for wt open,  $c_{20} = 1.85$ ,  $R_x = 10^{8.20} \text{ s}^{-1}$ ,  $R_y = 10^{7.90} \text{ s}^{-1}$ ,  $R_z = 10^{8.30} \text{ s}^{-1}$ ,  $\alpha_D = 14^\circ$ ,  $\beta_D = 43^\circ$ ,  $\gamma_D = 82^\circ$ , and  $\text{gib2} = 0.89$ ; for +5A,  $c_{20} = 1.30$ ,  $R_x = 10^{7.74} \text{ s}^{-1}$ ,  $R_z = 10^{8.08} \text{ s}^{-1}$ ,  $R_y = 10^{8.08} \text{ s}^{-1}$ ,  $\alpha_D = 28^\circ$ ,  $\beta_D = 50^\circ$ ,  $\gamma_D = 77^\circ$ , and  $\text{gib2} = 0.6$ .

## **S.II. Supplemental Results & Discussion**

### *S.II.A: Biochemical studies showed R5a does not perturb P1 docking*

The effect of R5a on P1 docking was assessed by measuring substrate dissociation from the wild type ribozyme, which proceeds in two steps: (i) undocking of the P1 duplex from the ribozyme core; and (ii) unwinding of the P1 duplex in the undocked state to release the oligonucleotide substrate (15). Although dissociation kinetics were followed, the results are expected to reflect thermodynamics of P1 docking because the docked state equilibrates prior to duplex unwinding (15,16) and, differences in docking equilibria have been shown to result from changes in the undocking and not the docking rate constant (17).

The experiments measured the ratio ( $k_{\text{rel}}$ ) between the  $k_{\text{off}}$  values for a pair of substrates (Table S3), with one favoring the docked state (at least for the wild type ribozyme; i.e.,  $rS_C$  or  $S_C^{\text{SL}}$ , Table S2) and the other favoring the undocked state (i.e.,  $rS_O$  or  $S_O^{\text{SL}}$ , Table S2). Each substrate pair has the same sequence and behaves the same in terms of simple helix stability. Therefore,  $k_{\text{rel}}$  reports exclusively on P1 undocking and not on properties of the open complex (18). The data showed identical values of  $k_{\text{rel}}$  in the presence and absence of R5a (Table S3). This result indicates that R5a does not perturb the P1 docking transition.

There is a 30-fold increase in the values of  $k_{\text{off}}$  for the spin labeled oligonucleotides ( $S_C^{\text{SL}}$  vs.  $rS_C$  and  $S_O^{\text{SL}}$  vs.  $rS_O$ ) (Table S3, I and II). This increase indicates R5a reduces duplex stability in the undocked state. Such destabilization arises from two modifications required for R5a labeling.

One is the deoxyadenosine placed at position +2 (+2dA), which has a 3-fold effect according to  $k_{off}$  measurements (Table S3, II and III). The other is the presence of R5a itself. Thermal denaturation measurements on the isolated P1 duplex gave a  $\Delta\Delta G^0_{50^\circ\text{C}}$  of 1.6 kcal/mol between  $S_C^{SL}$  and  $rS_C$ , corresponding to a 12-fold effect of duplex destabilization due to the presence of R5a. Together the presence of R5a and +2dA destabilized the duplex by 36-fold, in good agreement with the kinetic results shown in Table S3.

**Table S3: Rate constants for dissociation of oligonucleotides from the L-16 Scal ribozyme/substrate complex.**

	SUBSTRATE	$k_{off}$ ( $\text{min}^{-1}$ )	$k_{rel}$
I	$S_C^{SL}$	0.079	0.13
	$S_O^{SL}$	0.627	
II	$rS_C$	0.0026	0.13
	$rS_O$	0.020	
III	$S_C^{SL(-)}$	0.0083	0.13
	$S_O^{SL(-)}$	0.064	

*S.II.B: Unbound substrate oligonucleotides behave differently from those in the ribozyme complexes*

As shown in Figure S2, R5a labeled substrate oligonucleotides gave different EPR spectra as compared to that of the ribozyme complexes. Therefore, spectra obtained in the presence of ribozyme report features specific to the complex.

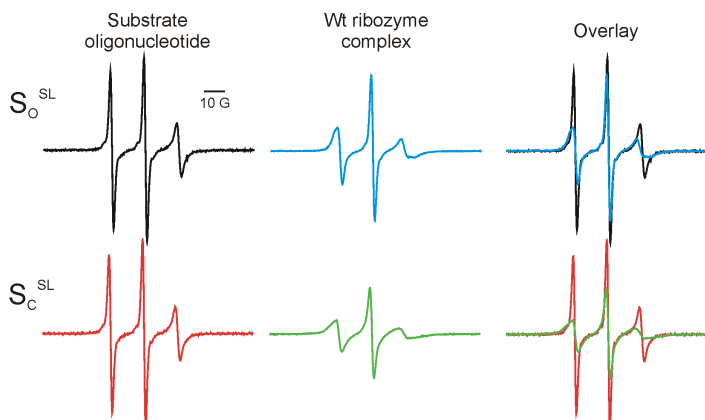


**Figure S2:** Comparison of EPR spectra of the individual oligonucleotides and those of the ribozyme complexes.

*S.II.C: The origin of R5a mobility reduction in the docked state*

The EPR spectrum of R5a is dictated by three modes of motions: (i) tumbling of the entire complex, characterized by a rotational correlation time  $\tau_R$ ; (ii) nitroxide internal motion ( $\tau_i$ ), which refers to rotational motions about the bonds connecting the pyrroline ring to the RNA; and (iii) local RNA motions ( $\tau_B$ ).

In our studies, the ~120 kD ribozyme complex has an estimated  $\tau_R$  of > 50 ns. Therefore, changes in the tumbling of the entire complex will not change the X-band EPR spectrum. Furthermore, the undocked state likely has a larger volume than the docked state. If P1 docking

affects complex tumbling at all, it will shorten  $\tau_R$ , leading to faster R5a motion. Therefore, docking induced R5a mobility reduction is not due to changes in overall tumbling of the complex.

Several lines of evidence indicate that P1 docking does not give rise to additional R5a/RNA contacts so that direct effects on nitroxide internal motion are unlikely. First, biochemical studies with the *Tetrahymena* intron suggest that the residues surrounding the spin label position make no tertiary interactions with the rest of the ribozyme (19,20). Indeed, the stability of the closed complex relative to the open complex is the same for P1 duplexes containing the cognate substrate and the R5a-labeled substrate (Table S3).

Second, we have measured EPR spectra of R5a attached to the  $R_P$  diastereomers of  $S_O^{SL}$  and  $S_C^{SL}$ , and compared them with data obtained from  $S_P$ -nitroxides described in the main text. The

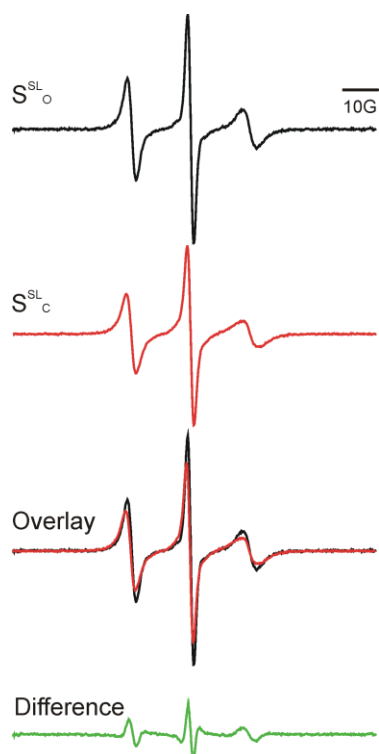


**Figure S4:** Spectra of wild type ribozyme complexes obtained using R5.

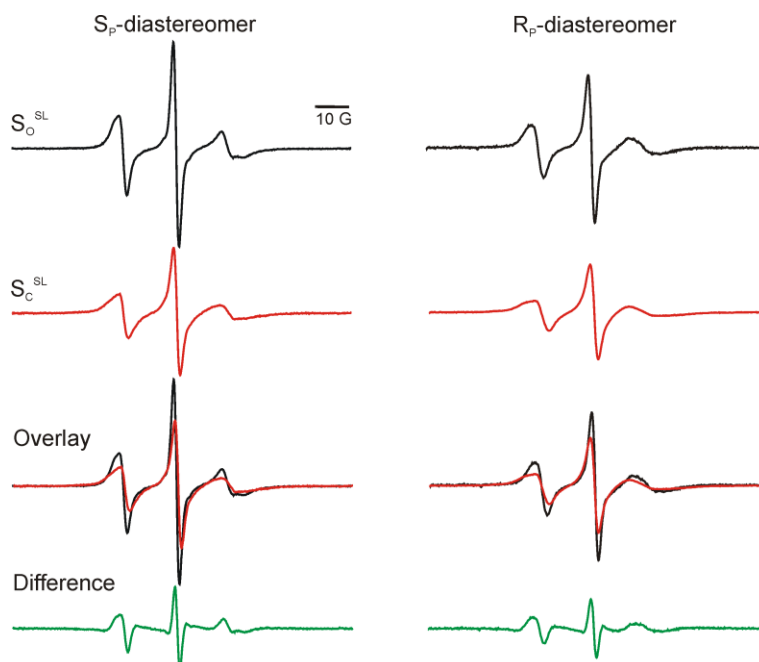
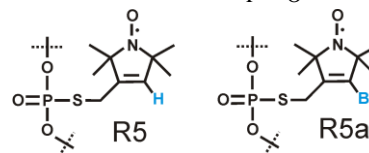


**Figure S3:** Comparison of spectra for wild type ribozyme complexes obtained using R5a attached to the  $S_P$  or the  $R_P$  phosphorothioate diastereomers.

$S_P$ - and  $R_P$ -diastereomers position the nitroxide to different locations, with the  $S_P$ -nitroxide directed towards solvent, while the  $R_P$ -nitroxide towards the duplex groove. Such spatial difference led to reduced R5a mobility in  $R_P$ - $S_O^{SL}$  as compared to  $S_P$ - $S_O^{SL}$  (Fig. S3). Importantly, the spectral difference between  $R_P$ - $S_O^{SL}$  and  $R_P$ - $S_C^{SL}$  is very similar to that between  $S_P$ - $S_O^{SL}$  and  $S_P$ - $S_C^{SL}$  (Fig. S3). If such spectral changes were due to additional R5a/RNA contacts in the docked state, one would conclude that a similar set of R5a/RNA contacts are present for the  $S_P$ - and  $R_P$ -nitroxides upon P1 docking. However, this is unlikely because the  $S_P$ -nitroxide occupies a different location than the  $R_P$ -nitroxide. Therefore, the similarity in docking induced spectral changes between the  $S_P$ -nitroxide and  $R_P$ -nitroxide argues against additional R5a/RNA contacts.



**Scheme S1**

Furthermore, the wild type ribozyme complexes were studied using a modified nitroxide probe, R5 (Fig. S4). R5 is attached to the RNA using the same chemical scheme as that of R5a (Scheme S1). In R5a, a 4-Br group is present at the pyrroline ring, which restricts torsional rotations about two out of the three bonds

connecting the pyrroline ring to RNA. These restrictions are released in R5 as a 4-H group replaces the 4-Br, leading to a higher degree of nitroxide internal motion and higher mobility of R5 as compared to R5a (compare Figs. S3 & S4). Both R5-S<sub>O</sub><sup>SL</sup> and R5-S<sub>C</sub><sup>SL</sup> gave spectra showing three narrow-lines with unequal amplitudes, which are characteristics of nitroxides undergoing fast rotations (Fig. S4). The R5-S<sub>C</sub><sup>SL</sup> spectrum is broader than that of R5-S<sub>O</sub><sup>SL</sup>, again indicating reduced nitroxide motion in the docked state (Fig. S4). If additional nitroxide/RNA contacts occur in the docked state, one would expect R5-S<sub>C</sub><sup>SL</sup> showed extra spectral component(s) due to the presence of low mobility R5 populations. There is no indication at all of such low mobility populations in the data (Fig. S4). Therefore, the R5 data also supports a lack of docking induced additional nitroxide/RNA contacts.

As we exclude changes in global tumbling of the complex and the internal motions of nitroxide, the observed R5a mobility reduction in the docked state is attributed to changes in RNA local motions. The P1 duplex acts as a unit during docking, and its dynamics will transmit to the labeling site and modulate R5a motion. An alternative scenario is that R5a is not sensing dynamic changes of the entire duplex unit, but only of the nucleotide at which R5a is attached or those immediately surrounding it. This is unlikely, as again the residues surrounding the spin label position do not contact the rest of the intron (see above). Furthermore, spectral changes in response to J1/2 mutations, which are distal from the R5a attachment point, also support the conclusion that R5a reports motion of the entire P1 duplex.

The analyses provide strong evidence that R5a mobility reduction in the docked state arise from changes in the dynamics of the P1 duplex.

#### *S.II.D: Mutant ribozymes favor the undocked state*

Figure S5 compares spectra between various ribozyme complexes. For the S<sub>O</sub><sup>SL</sup> substrate, which directs the wild type (wt) ribozyme to the undocked state, spectral differences are small for the wt/-3A pair and the wt/+5A pair, respectively (Fig. S5A). For the S<sub>C</sub><sup>SL</sup> substrate, which directs the wild-type ribozyme to the docked state, spectra differences are large for the wt/-3A pair and the wt/+5A pair (Fig. S5B). In addition, S<sub>C</sub><sup>SL</sup> spectra for both ribozyme mutants show sharper lines than that of the wt ribozyme, indicating higher nitroxide mobility (Fig. S5B). Taken

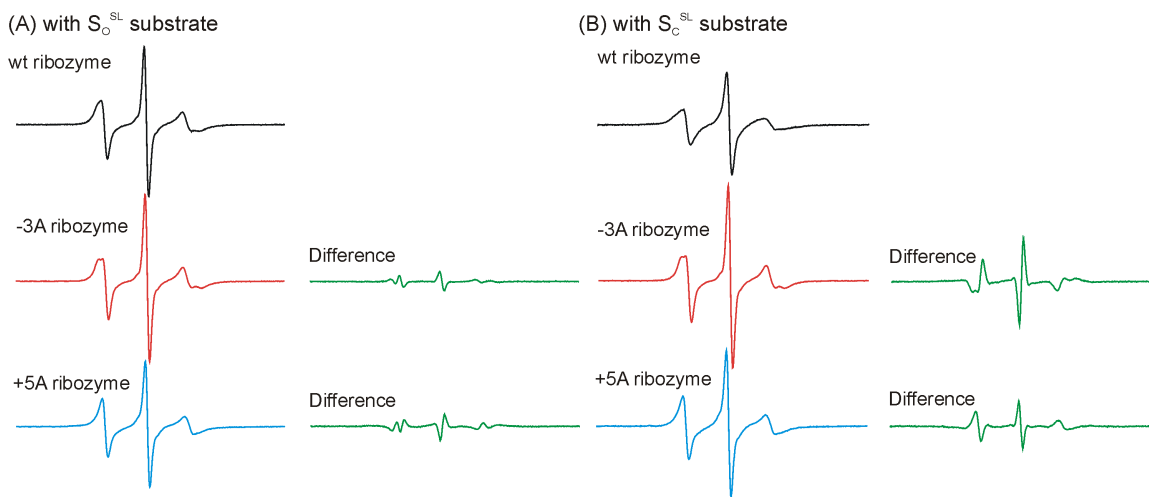


**Figure S5:** Spectral comparison between mutant and wild type ribozyme complexes. In each panel, difference spectra were obtained by subtracting the “wt ribozyme” spectrum from that of the corresponding mutant ribozyme.

together, the data show that with the -3A and the +5A ribozyme, the nitroxide has a high mobility that is similar to that of the undocked state of the wt ribozyme. Within the resolution of the EPR data, both mutant ribozymes show no evidence of docking. Therefore, both favor the undocked state. This agrees with previous, more direct measures of docking with these mutant ribozymes (15,21) (L.E. Bartley & DH, unpublished data).

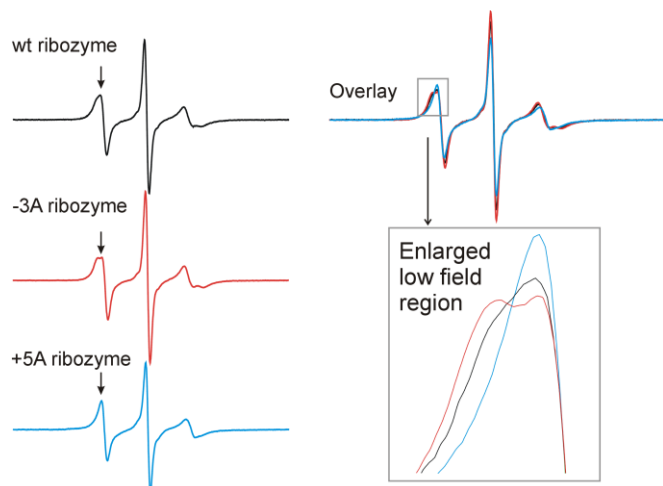
*S.II.E: Variations in the spectra of mutant ribozyme complexes reveal differences in the undocked state*

Figure S6 compares spectra for various ribozymes obtained using the  $S_0^{SL}$  substrate. Differences can be clearly observed at the overlay panel.

*S.II.F: EPR spectral simulations*

Simulations were carried out using the MOMD program, which uses an order parameter ( $S$ ) and an effective correlation time ( $\tau$ ) to describe the nitroxide diffusive motion (see Methods). It is known that in MOMD simulations certain parameters, such as  $S$  and  $\tau$ , may be correlated and not uniquely determined (8-10). For example, within a certain range, the effect of a larger  $S'$  (a more restricted potential,  $S' > S$ ) may often be compensated by a smaller  $\tau'$  (faster rate, as  $\tau \propto 1/\text{rate}$ ), so that  $(S, \tau)$  and  $(S', \tau')$  give simulated spectra that fit equally well to the experimental data.

To assess the influence of  $S/\tau$  co-variation, simulations were carried out at a fixed  $\tau$  (Fig. S7). The simulated spectra fit the respective experimental data well, although the degree of agreement is slightly worse than those obtained with fitting both  $S$  and  $\tau$  (Fig. 2 in text). The fixed  $\tau$  simulations show the same trend of decreasing motional restriction (decreasing  $S$ ) as  $J1/2$  is extended. Therefore,  $S/\tau$  co-variation does not change our conclusions on how  $J1/2$  mutations affect P1 duplex motion.



**Figure S6:** Comparisons of ribozyme complex spectra obtained with the  $S_0^{SL}$  substrate.

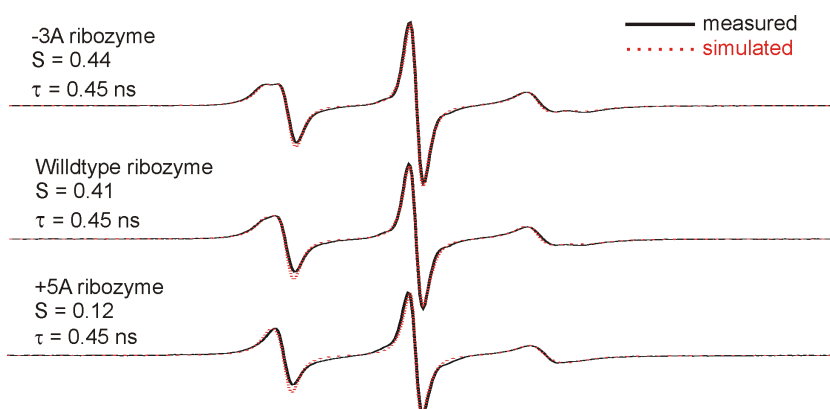


**Figure S7:** Spectral simulations using a fixed rate. Simulations used fixed nitroxide diffusion rotation rates ( $R_x = 10^{8.51} \text{ s}^{-1}$ ,  $R_y = 10^{8.22} \text{ s}^{-1}$ , and  $R_z = 10^{7.95} \text{ s}^{-1}$ ) that give an overall  $\tau = 0.45 \text{ ns}$ . The final values for the variable parameters are: for -3A,  $c_{20} = 2.01$ ,  $\alpha_D = 2.80^\circ$ ,  $\beta_D = 43.0^\circ$ ,  $\gamma_D = 53.4^\circ$ , and  $\text{gib2} = 1.0$ ; for wt open,  $c_{20} = 1.87$ ,  $\alpha_D = 7.49^\circ$ ,  $\beta_D = 42.0^\circ$ ,  $\gamma_D = 81.0^\circ$ , and  $\text{gib2} = 0.89$ ; for +5A,  $c_{20} = 0.57$ ,  $\alpha_D = 358.0^\circ$ ,  $\beta_D = 24.8^\circ$ ,  $\gamma_D = 87.4^\circ$ , and  $\text{gib2} = 0.0$ .

## References:

1. Karbstein, K., Lee, J. and Herschlag, D. (2007) Probing the Role of a Secondary Structure Element at the 5'- and 3'-Splice Sites in Group I Intron Self-Splicing: The Tetrahymena L-16 ScaI Ribozyme Reveals a New Role of the G/U Pair in Self-Splicing. *Biochemistry*, **46**, 4861-4875.
2. Zaug, A.J., Kent, J.R. and Cech, T.R. (1985) Reactions of the intervening sequence of the Tetrahymena ribosomal ribonucleic acid precursor: pH dependence of cyclization and site-specific hydrolysis. *Biochemistry*, **24**, 6211-6218.
3. Zaug, A.J., Kent, J.R. and Cech, T.R. (1984) A labile phosphodiester bond at the ligation junction in a circular intervening sequence RNA. *Science*, **224**, 574-578.
4. Grant, G.P.G., Popova, A. and Qin, P.Z. (2008) Diastereomer characterizations of nitroxide-labeled nucleic acids. *Biochem. Biophys. Res. Commun.*, **371**, 451-455.
5. Qin, P.Z., Jennifer, I. and Oki, A. (2006) A model system for investigating lineshape/structure correlations in RNA site-directed spin labeling. *Biochem. Biophys. Res. Commun.*, **343**, 117-124.
6. Karbstein, K., Carroll, K.S. and Herschlag, D. (2002) Probing the Tetrahymena Group I Ribozyme Reaction in Both Directions. *Biochemistry*, **41**, 11171-11183.
7. Mei, R. and Herschlag, D. (1996) Mechanistic Investigations of a Ribozyme Derived from the Tetrahymena Group I Intron: Insights into Catalysis and the Second Step of Self-Splicing. *Biochemistry*, **35**, 5796-5809.
8. Budil, D.E., Lee, S., Saxena, S. and Freed, J.H. (1996) Nonlinear-least-squares analysis of slow-motion EPR spectra in one and two dimensions using a modified Levenberg-Marquardt algorithm. *J. Mag. Res. Series A*, **120**, 155-189.
9. Earle, K.A. and Budil, D., E. (2006) In Schlick, S. (ed.), *Advanced ESR Methods in Polymer Research*. John Wiley and Sons, New York.
10. Columbus, L., Kalai, T., Jeko, J., Hideg, K. and Hubbell, W.L. (2001) Molecular motion of spin-labeled side chains in  $\alpha$ -helices: analysis by variation of side chain structure. *Biochemistry*, **40**, 3828-3846.
11. Qin, P.Z., Hideg, K., Feigon, J. and Hubbell, W.L. (2003) Monitoring RNA base structure and dynamics using site-directed spin labeling. *Biochemistry*, **42**, 6772-6783.
12. Kim, N.K., Murali, A. and DeRose, V.J. (2005) Separate metal requirements for loop interactions and catalysis in the extended hammerhead ribozyme. *J. Am. Chem. Soc.*, **127**, 14134-14135.
13. Liang, Z., Freed, J.H., Keyes, R.S. and Bobst, A.M. (2000) An electron spin resonance study of DNA dynamics using the slowly relaxing local structure model. *J. Phys. Chem.*, **104**, 5372-5381.
14. Budil, D.E., Sale, K.L., Khairy, K.A. and Fajer, P.G. (2006) Calculating slow-motional electron paramagnetic resonance spectra from molecular dynamics using a diffusion operator approach. *J Phys. Chem. A*, **110**, 3703-3713.
15. Herschlag, D. (1992) Evidence for processivity and two-step binding of the RNA substrate from studies of J1/2 mutants of the Tetrahymena ribozyme. *Biochemistry*, **31**, 1386-1399.
16. Narlikar, G.J., Bartley, L.E., Khosla, M. and Herschlag, D. (1999) Characterization of a Local Folding Event of the Tetrahymena Group I Ribozyme: Effects of Oligonucleotide Substrate Length, pH, and Temperature on the Two Substrate Binding Steps. *Biochemistry*, **38**, 14192-14204.

17. Bartley, L.E., Zhuang, X., Das, R., Chu, S. and Herschlag, D. (2003) Exploration of the Transition State for Tertiary Structure Formation between an RNA Helix and a Large Structured RNA. *Journal of Molecular Biology*, **328**, 1011-1026.
18. Narlikar, G.J., Khosla, M., Usman, N. and Herschlag, D. (1997) Quantitating Tertiary Binding Energies of 2' OH Groups on the P1 Duplex of the Tetrahymena Ribozyme: Intrinsic Binding Energy in an RNA Enzyme. *Biochemistry*, **36**, 2465-2477.
19. Karbstein, K. and Herschlag, D. (2003) Extraordinarily slow binding of guanosine to the Tetrahymena group I ribozyme: Implications for RNA preorganization and function. *Proceedings of the National Academy of Sciences of the United States of America*, **100**, 2300-2305.
20. Hougland, J.L., Piccirilli, J.A., Forconi, M., Lee, J. and Herschlag, D. (2006) In Gesteland, R. F., Cech, T. R. and Atkins, J. F. (eds.), *The RNA World*. 3rd ed. Cold Spring Harbor Laboratory Press, Cold Spring Harbor, New York, pp. 133-201.
21. Young, B., Herschlag, D. and Cech, T.R. (1991) Mutations in a nonconserved sequence of the Tetrahymena ribozyme increase activity and specificity. *Cell*, **67**, 1007-1019.